

Compressibility and speeds of sound across the superfluid to supersolid phase transition of an elongated dipolar gas

P. B. Blakie,^{1,2} L. Chomaz,³ D. Baillie,^{1,2} and F. Ferlaino^{4,5}

¹*Dodd-Walls Centre for Photonic and Quantum Technologies, New Zealand*

²*Department of Physics, University of Otago, Dunedin 9016, New Zealand*

³*Physikalisches Institut der Universität Heidelberg, Im Neuenheimer Feld 226, 69120 Heidelberg, Germany*

⁴*Institut für Experimentalphysik, Universität Innsbruck, Technikerstraße 25, 6020 Innsbruck, Austria*

⁵*Institut für Quantenoptik und Quanteninformation, Österreichische Akademie der Wissenschaften, Technikerstraße 21a, 6020 Innsbruck, Austria*

(Dated: June 9, 2023)

We investigate the excitation spectrum and compressibility of a dipolar Bose-Einstein condensate in an infinite tube potential in the parameter regime where the transition between superfluid and supersolid phases occurs. Our study focuses on the density range in which crystalline order develops continuously across the transition. Above the transition the superfluid shows a single gapless excitation band, phononic at small momenta and with a roton at a finite momentum. Below the transition, two gapless excitation branches (three at the transition point) emerge in the supersolid. We examine the two gapless excitation bands and their associated speeds of sound in the supersolid phase. Our results show that the speeds of sound and the compressibility are discontinuous at the transition, indicating a second-order phase transition. These results provide valuable insights into the identification of supersolid phenomena in dipolar quantum gases and the relationship to supersolidity in spin-orbit coupled gases.

I. INTRODUCTION

Experiments with dipolar Bose-Einstein condensates (BECs) have observed the transition to a supersolid ground state [1–3], and have studied its elementary excitations [4–6]. The supersolid state breaks translational invariance by developing a spatially modulated (crystalline) structure, while still exhibiting superfluidity. For a D -dimensional crystal the supersolid state will exhibit $D + 1$ gapless excitation branches. These reflect the number of Nambu-Goldstone modes associated with the spontaneously broken symmetries of the supersolid state [7]. The excitations can be classified by the character of fluctuations they cause [6, 8, 9]. Although there is hybridization of the properties of the branches, D of the gapless branches are generally associated with density fluctuations and are termed density or phonon branches. The remaining gapless branch of excitations is associated with phase fluctuations and is referred to as a phase or Bogoliubov branch, related to superfluid aspects of the system (i.e. tunneling of atoms between unit cells).

The majority of recent experimental work with dipolar BECs have used cigar shaped potentials in which a $D = 1$ supersolid transition can occur. The relevant thermodynamic limit of this system is an infinitely long tube trap, i.e. a system with transverse confinement only and a fixed linear density [10–14] [see Fig. 1(a)]. It is found that, depending on the density, the supersolid transition in the thermodynamic system can be continuous or discontinuous [12–14]. The continuous transition emerges for a range of intermediate densities, and occurs when a roton excitation gap of the uniform BEC state vanishes [10, 12, 13] [see Fig. 1(b)]. Experimental and theoretical studies of the finite system also reveal similar behavior (e.g. see [15–17]). It has also been shown that two gapless excitation branches (a density and a phase branch) emerge in the transition to the 1D supersolid state [4–6, 10, 13, 18]. We note that in the finite sized experimental systems the super-

solid transition is revealed by a bifurcation in the compressional excitations of the gas [4, 6], which can be interpreted as in-phase and out-of-phase combinations of the gapless excitations of the thermodynamic system.

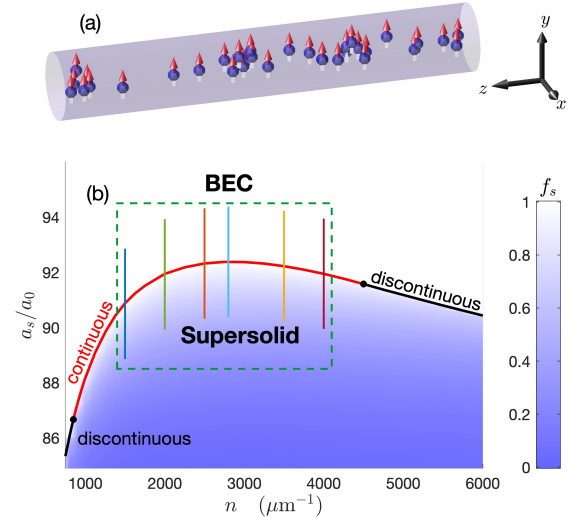


FIG. 1. (a) Schematic figure of thermodynamic system: infinite tube-shaped potential confining dipoles polarized along y . (b) Phase diagram showing the superfluid fraction of the ground state as a function of density n and the s -wave scattering length a_s . The uniform BEC (superfluid) and modulated supersolid states are shown separated by a continuous (red line) or discontinuous (black line) transition. Dashed box indicates the parameter regime we consider in this work, focusing on the continuous transition. Vertical colored lines show the parameter regime for the transition data considered in Fig. 4(a). Phase diagram for ^{164}Dy using $a_{\text{dd}} = 130.8 a_0$ and with $\omega_\rho = 2\pi \times 150$ Hz (see [14]).

We also note studies of supersolid properties in the ther-

modynamic regime for bosons with dipole-dipole interactions (DDIs) with $D = 2$ [19, 20] or general soft-core interactions with $D = 1$ [21], $D = 2$ [8, 22–25], or $D = 3$ [9, 22, 26]. For the $D = 1$ soft-core system the transition is always continuous¹. For the $D > 1$ cases the transition to the supersolid state is generally first order² and the system properties change abruptly at the transition.

Spin-orbit coupled BECs also exhibit a phase transition to a supersolid-like stripe phase, which has been observed in experiments [27]. For this realization the coupling to an optical field produces a $D = 1$ (supersolid) stripe phase (irrespective of system dimension) and two gapless excitation branches are predicted [28]. The transition from the uniform planewave phase to the stripe phase is first-order [29, 30], in contrast to the $D = 1$ soft-core case and the dipolar case at intermediate densities [Fig. 1(b)]. Features of the spin-orbit system, such as the speeds of sound and compressibility in the thermodynamic regime, have been theoretically studied across the transition [28, 30, 31]. These features remain unexplored for the $D = 1$ dipolar supersolid. We address this here by examining the behaviour of the excitations, speeds of sound, density response, and compressibility of this system. We focus on the parameter regime where the crystalline order develops continuously [see Fig. 1(b)] and find that the compressibility and the speeds of sound change discontinuously across this transition. Thus indicating that the transition is second order.

II. SYSTEM AND GROUND STATES

Here we consider a gas of magnetic bosonic atoms in a radially symmetric tube potential $V = \frac{1}{2}m\omega_\rho(x^2 + y^2)$, where ω_ρ is the angular trap frequency describing the transverse confinement. The theoretical description of this system is provided by an extended Gross-Pitaevskii equation (eGPE) which includes the leading order effects of quantum fluctuations [32–35], and has been extensively used to model supersolid experiments with dipolar BECs (e.g. see [1–3]). The eGPE energy functional for this system is

$$E = \int d\mathbf{x} \psi^* \left[h_{\text{sp}} + \frac{1}{2}g_s|\psi|^2 + \frac{1}{2}\Phi_{\text{dd}} + \frac{2}{5}\gamma_{\text{QF}}|\psi|^3 \right] \psi, \quad (1)$$

where $h_{\text{sp}} = -\frac{\hbar^2}{2m}\nabla^2 + V$ is the single particle Hamiltonian. The short ranged interactions are governed by the coupling constant $g_s = 4\pi\hbar^2 a_s/m$ where a_s is the s -wave scattering length. The long-ranged DDIs are described by the potential

$$\Phi_{\text{dd}}(\mathbf{x}) = \int d\mathbf{x}' U_{\text{dd}}(\mathbf{x} - \mathbf{x}') |\psi(\mathbf{x}')|^2, \quad (2)$$

where the atoms are polarized along y with $U_{\text{dd}}(\mathbf{r}) = \frac{3g_{\text{dd}}}{4\pi r^3} (1 - 3y^2/r^2)$. Here $g_{\text{dd}} = 4\pi\hbar^2 a_{\text{dd}}/m$, with $a_{\text{dd}} = m\mu_0\mu_m^2/12\pi\hbar^2$ being the dipolar length, and μ_m the atomic magnetic moment. The effects of quantum fluctuations are described by the quintic nonlinearity with coefficient $\gamma_{\text{QF}} = \frac{32}{3}g_s\sqrt{a_s^3/\pi}Q_5(\epsilon_{\text{dd}})$ where $Q_5(x) = \Re\{\int_0^1 du [1 + x(3u^2 - 1)]^{5/2}\}$ [36] and $\epsilon_{\text{dd}} \equiv a_{\text{dd}}/a_s$.

We constrain the stationary states of Eq. (1) to have an average linear density of n , and ground states are found (following Ref. [14]) by minimising the energy per particle. For the case of modulated (crystalline) states, the system chooses a preferred unit cell size L , and the normalization constraint is $\int_{\text{uc}} dz \int d\boldsymbol{\rho} |\psi|^2 = nL$, where $\boldsymbol{\rho} = (x, y)$ represents the transverse coordinates, and uc denotes the unit cell $z \in [-\frac{1}{2}L, \frac{1}{2}L]$. These stationary states are solutions of the eGPE

$$\mu\psi = (h_{\text{sp}} + g_s|\psi|^2 + \Phi_{\text{dd}} + \gamma_{\text{QF}}|\psi|^3) \psi, \quad (3)$$

where μ is the chemical potential.

In Fig. 2 we present results illustrating the transition from a uniform to spatially modulated state as the s -wave scattering length is reduced. For the parameters considered in these results the ground state is uniform (superfluid state) for $a_s > a_{\text{rot}} = 92.32 a_0$. Here a_{rot} is the value of the scattering length where a roton excitation goes soft as we will discuss in Sec. III (also see [10, 11]). For $a_s < a_{\text{rot}}$ the ground state is modulated. We can characterise the strength of modulation using the density contrast

$$\mathcal{C} = \frac{n_{\text{max}} - n_{\text{min}}}{n_{\text{max}} + n_{\text{min}}}, \quad (4)$$

where n_{max} and n_{min} are the maximum and minimum of the linear density $n(z) = \int d\boldsymbol{\rho} |\psi|^2$, respectively. Results for \mathcal{C} show that the density modulation develops continuously as a_s decreases below a_{rot} [see Fig. 2(b)-(d), Fig. 3(a), and Refs. [10, 12–14]].

III. EXCITATIONS

The elementary quasi-particle excitations are described within the framework of Bogoliubov theory. In this theory the excitations give the small deviations of the condensate field with respect to ground state as

$$\Psi(\mathbf{x}, t) = e^{-i\mu t/\hbar} \left[\psi(\mathbf{x}) + \sum_{\nu, q_z} \left\{ c_{\nu, q_z} u_{\nu, q_z}(\mathbf{x}) e^{-i\omega_{\nu, q_z} t} - c_{\nu, q_z}^* v_{\nu, q_z}^*(\mathbf{x}) e^{i\omega_{\nu, q_z}^* t} \right\} \right]. \quad (5)$$

Here $\epsilon_{\nu, q_z} = \hbar\omega_{\nu, q_z}$ are the quasi-particle energies, $\hbar q_z$ is a quasi-momentum in the first Brillouin zone, i.e. $q_z \in [-\pi/L, \pi/L]$, ν is the band index and c_{ν, q_z} are the expansion amplitudes. The quasi-particle amplitudes take the Bloch form

$$u_{\nu, q_z}(\mathbf{x}) = \bar{u}_{\nu, q_z}(\mathbf{x}) e^{iq_z z}, \quad v_{\nu, q_z}(\mathbf{x}) = \bar{v}_{\nu, q_z}(\mathbf{x}) e^{iq_z z}, \quad (6)$$

¹ The discontinuous regime for the $D = 1$ tube confined dipolar BEC emerges from the three-dimensional character of the system

² There is a critical point for the $D = 2$ DDI case where the transition is continuous at particular critical density [20].

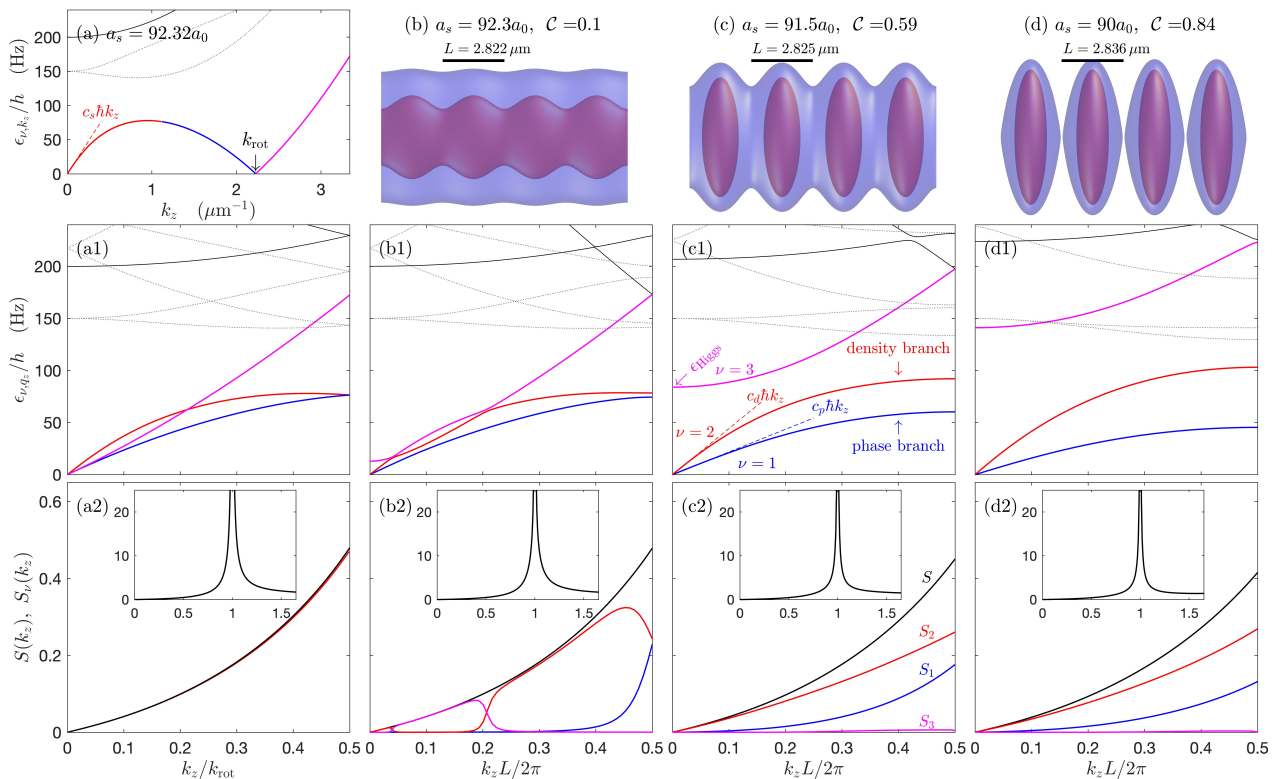


FIG. 2. Density profiles, excitation spectra and structure factors of a dipolar Bose gas in an infinite tube. (a) Excitation spectrum for a uniform system at $a_s = a_{\text{rot}}$ where the roton softens. Excitations bands with even parity in x and y (solid lines), other bands (dotted lines). (a1) The results from (a) reduced to the first Brillouin zone with the colours of the lowest 3 even symmetry bands corresponding to the segments in (a). (a2) The static structure factor $S(k_z)$ (black line) is dominantly contributed by the lowest band of (a) [i.e. $S_1(k_z)$, red line for the k_z range considered] (see Sec. V). Inset shows $S(k_z)$ over a wider momentum range. (b)-(d) Density isosurfaces of crystalline ground states for $a_s < a_{\text{rot}}$. Red (blue) isosurface at $4 \times 10^{20} \text{ m}^{-3}$ (10^{20} m^{-3}). Unit cell size L and density contrast C are also indicated. The excitation spectra (b1)-(d1) and static structure factors (b2)-(d2) corresponding to the ground states in (b)-(d), using same line types as in (a1) and (a2), respectively. The static structure factor is shown (black line) and individual contributions of the lowest three excitations bands (i.e. $S_{\nu=1,2,3}$) [see labels in (c2)]. Results for ^{164}Dy using $a_{\text{dd}} = 130.8 a_0$ for a linear density of $n = 2500 \mu\text{m}^{-1}$ and with $\omega_\rho = 2\pi \times 150\text{Hz}$.

where $\{\bar{u}_{\nu, q_z}(\mathbf{x}), \bar{v}_{\nu, q_z}(\mathbf{x})\}$ are periodic in the unit cell. More details of the Bogoliubov analysis of the eGPE can be found in Ref. [37].

In Fig. 2 we show some examples of the excitation spectra of the system. The case in Fig. 2(a) is for a uniform state at the transition point $a_s = a_{\text{rot}}$. Here the z -momentum $\hbar k_z$ is a good quantum number for the excitations³. A single Nambu-Goldstone branch exists in the uniform state, corresponding to the lowest energy excitation band that is gapless as $k_z \rightarrow 0$. This reflects the broken gauge symmetry associated with superfluidity. We observe a fully developed roton-like local minimum in the excitation spectrum that has softened to zero energy. Here we define a_{rot} as the value of a_s where the roton feature of the uniform state has a minimum at zero-energy (i.e. a fully softened roton). We note that a_{rot} varies with n and confinement. The wavevector of the softened roton is denoted k_{rot} and the density modulation first develops at the transition point with a unit cell size set by the roton wave-

length, i.e. as $a_s \rightarrow a_{\text{rot}}$ from below, $L \rightarrow 2\pi/k_{\text{rot}}$. To aid in our later comparison to the excitations of the modulated ground states, in Fig. 2(a1) we map the uniform state excitation results of subplot (a) onto the positive part of first Brillouin zone ($q_z \in [-\frac{1}{2}k_{\text{rot}}, \frac{1}{2}k_{\text{rot}}]$), taking k_{rot} as the reciprocal lattice vector. The color coding of segments of the lowest excitation band used in (a) is selected to help identify the features in the reduced zone scheme. In particular, we note that the soft roton feature manifests in the reduced zone representation as 2 additional gapless excitations bands (blue and magenta color).

In Figs. 2(b1)-(d1) we show the excitation spectra corresponding to the modulated ground states shown in (b)-(d), respectively. The case in (b1) is close to the transition with a weak modulation. Here the spectrum is similar to the roton case [cf. (a1)], but the ground state modulation causes some noticeable changes in the lowest three excitations bands: a gap (for $q_z \rightarrow 0$) develops in the $\nu = 3$ (magenta color) band as we move away from the transition, while the other two bands remain gapless, and avoided crossings occur where the $\nu = 2$ (red color) and $\nu = 3$ (magenta color) bands approach each

³ In the uniform case we can take $q_z = k_z$, due to translational invariance.

other. For the more strongly modulated cases (c1) and (d1), the three lowest excitation bands separate, and can be unambiguously assigned. We denote the lowest gapless band (blue color) as the phase band, and the higher gapless band (red color) as the density band [see Fig. 2(c1)]. The identification of these bands can be made by assessing the dominant effect of the excitations on the phase or density fluctuations of the system as has been done for dilute supersolid states with soft-core interactions and DDIs (e.g. see [6, 8, 9]). In the spin-orbit coupled stripe phase, similarly two gapless bands emerge, but these are identified as spin and density nature, due to their effect on density and spin fluctuations [28].

IV. SUPERFLUIDITY, CHARACTERISTIC EXCITATIONS AND SPEEDS OF SOUND

In Fig. 3 we consider characteristic properties of the system across the transition. Subplot (a) shows both the density contrast and the superfluid fraction. We can view the contrast as an order parameter for the crystalline order of the system. The finite superfluid fraction in the modulated state confirms that the system is in a supersolid state. Note that here we have taken the superfluid fraction as the average of the upper and lower bounds developed by Leggett and given by the expressions

$$f_s^+ = \frac{L}{n} \left[\int_{uc} \frac{dz}{\int d\rho |\psi|^2} \right]^{-1}, \quad (7)$$

$$f_s^- = \frac{L}{n} \int d\rho \left[\int_{uc} \frac{dz}{|\psi|^2} \right]^{-1}, \quad (8)$$

respectively [38]. These two bounds typically differ by less than a percent from each other and are in good agreement the superfluid fraction obtained from the direct calculation of the nonclassical translational inertia of the system (see [14]).

We also consider the behavior of two characteristic excitations which reveal the approach to the transition from either side. In the uniform state the roton excitation plays this role and we define ϵ_{rot} as the energy of the local minimum in the rotonic feature (e.g. see [11]). As a_s approaches a_{rot} from above $\epsilon_{\text{rot}} \rightarrow 0$. The softening of this mode leads to a dynamic instability causing the formation of spatial modulation [16, 39]. In the modulated ground state a Higgs-like amplitude mode plays a key role in signifying the approach of the transition. The identification of Higgs-like mode is made with the $q_z \rightarrow 0$ part of the third excitation band, because these excitations cause amplitude fluctuations of the crystalline order [15]. Here we define $\epsilon_{\text{Higgs}} = \epsilon_{3, q_z=0}$ [see Fig. 2(c1)], and as a_s approaches a_{rot} from below $\epsilon_{\text{Higgs}} \rightarrow 0$, and the modulated order disappears. The inset to Fig. 3(b) reveals that the roton and Higgs energies both soften with an exponent of $\frac{1}{2}$, i.e. $\epsilon \sim \sqrt{|a_s - a_{\text{rot}}|}$, on their respective sides of the transition, consistent with the normal meanfield behaviour of the energy gap at a quantum phase transition [40].

Speeds of sound can be associated with the gapless excitation branches. The slope of the lowest band near $k_z = 0$ in the uniform phase identifies the usual Bogoliubov sound for a

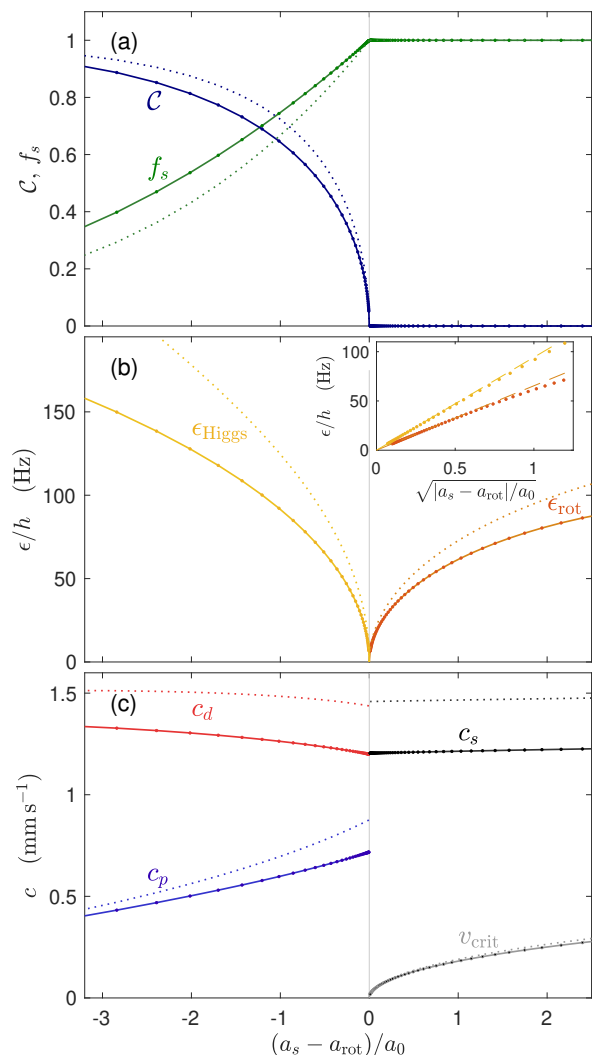


FIG. 3. Continuous transition between the uniform and modulated states at $n = 2.5 \times 10^3 \mu\text{m}^{-1}$ with $a_{\text{rot}} = 92.32 a_0$. (a) Density contrast and superfluid fraction, (b) the energy of roton and Higgs mode, and (c) speeds of sound and critical velocity in the uniform state. The inset to (b) shows that the modes soften as $\sim \sqrt{|a_s - a_{\text{rot}}|}$ in the approach to the transition, with the dashed lines being a linear fit to the data close to the transition. Small circles are results of our general 3D calculations and are fit with a solid line, except in the inset to (b) where these results are shown as small circles. For comparison the dotted lines show results of the reduced 3D theory where $a_{\text{rot}} = 90.56 a_0$. Other parameters as in Fig. 2.

BEC as [see Fig. 2(a)]

$$c_s = \frac{1}{\hbar} \left(\frac{\partial \epsilon_{1, k_z}}{\partial k_z} \right)_{k_z \rightarrow 0}. \quad (9)$$

Similarly, in the modulated phase the two lowest bands can be

used to define

$$c_p = \frac{1}{\hbar} \left(\frac{\partial \epsilon_{1,q_z}}{\partial q_z} \right)_{q_z \rightarrow 0}, \quad (10)$$

$$c_d = \frac{1}{\hbar} \left(\frac{\partial \epsilon_{2,q_z}}{\partial q_z} \right)_{q_z \rightarrow 0}, \quad (11)$$

as the phase and density speeds of sound, respectively [see Fig. 2(c1)]. Results for the speeds of sound are shown in Fig. 3(c). The speeds are seen to change discontinuously across the transition, and is the basis of our identification of the transition as being second order⁴. For the density we consider here the discontinuity is rather small with c_d and c_s being almost equal at the transition point [see Fig. 4(c) for an example at a lower density where the discontinuity is larger]. The discontinuity in the speeds of sound arises from the avoided crossing between the low energy bands [e.g. see Fig. 2(b1)]. As we approach the transition from below the avoided crossing shifts towards $k_z \rightarrow 0$ and hence affects the speeds of sound at the transition. We also note that the two speeds of sound in the stripe phase of spin-orbit coupled BEC have been identified and studied in Refs. [28, 31].

We also show the critical velocity in the uniform state evaluated using the Landau criteria

$$v_{\text{crit}} = \min_{k_z} \left(\frac{\epsilon_{1,k_z}}{\hbar k_z} \right). \quad (12)$$

For a_s close to the transition the critical velocity is approximately given by $v_{\text{crit}} \approx \epsilon_{\text{rot}}/\hbar k_{\text{rot}}$ [41], and the softening of the roton causes it to go to zero. The critical velocity and dynamics flow past an obstacle has been studied in soft-core models of supersolids [22, 25, 42], but we have not made any extension of those ideas to our system.

While our main results in this paper are obtained by full numerical calculations, in Fig. 3 we also show the results of the reduced 3D theory [11–13]. The reduced theory makes a variational description of the transverse degrees of freedom, and reduces the calculation to an effective one-dimensional model. In general the reduced theory produces qualitatively comparable results, although the speed of sound (particularly c_s and c_d) tends to be significantly over estimated. This over-estimation was also discussed in the context of the uniform state study presented in Ref. [43]. These results suggest some caution is require in using reduced theory as a quantitative description of the system excitations.

V. STRUCTURE FACTORS AND COMPRESSIBILITY

In addition to the spectrum of the excitations our interest here extends to the nature of the density fluctuations of the system, and their connection to compressibility. We can make

this connection via the dynamical structure factor, which determines the response of the system to a density coupled probe, where the probe transfers momentum $\hbar \mathbf{k}$ and energy $\hbar \omega$ to the system. For the case of a momentum along the z -axis (i.e. tube axis) and the dynamic structure factor of the $T = 0$ system is [44, 45]

$$S(k_z, \omega) = \sum_{\nu} |\delta n_{\nu, k_z}|^2 \delta(\hbar \omega - \hbar \omega_{\nu, q_z}), \quad (13)$$

where

$$\delta n_{\nu, k_z} = \int_{\text{uc}} dz \int d\rho [u_{\nu, q_z}^*(\mathbf{x}) - v_{\nu, q_z}^*(\mathbf{x})] e^{ik_z z} \psi(\mathbf{x}). \quad (14)$$

In this expression, and others where both k_z and q_z appear, the value of quasimomentum q_z is fixed by k_z reduced to the first Brillouin zone by an integer number of reciprocal lattice vectors $2\pi/L$ (also see [46]). It is possible to measure the dynamic structure factor in cold-atom experiments using Bragg spectroscopy, which has been used to probe excitation properties of dipolar BECs [18, 47, 48]. Here our main interest lies in the static structure factor is given by

$$S(k_z) \equiv \frac{\hbar}{nL} \int d\omega S(k_z, \omega). \quad (15)$$

This can also be directly measured using high resolution *in situ* imaging of the density fluctuations, e.g. for the dipolar case see Refs. [16, 49]. The static structure factor over a broad momentum range is shown in the insets of Figs. 2(a2)-(d2). Here a divergence occurs at reciprocal lattice vector reflecting the periodic structure of the ground state⁵. We can examine the contribution from each band to the structure factor, i.e. setting $S(k_z) = \sum_{\nu} S_{\nu}(k_z)$, where $S_{\nu}(k_z) = \frac{1}{nL} |\delta n_{\nu, k_z}|^2$ is the contribution from the ν -band. Results focusing on $S(k_z)$ and $S_{\nu}(k_z)$ for low values of k_z and $\nu = 1, 2, 3$, are shown (a2)-(d2). The contributions of higher bands ($\nu > 3$) are negligible. The avoided crossings in the spectrum (b1) are revealed in the behavior of the S_{ν} in (b2), where the weight smoothly transfers between the bands at the avoided crossings. For the cases (c1,d1) where the lowest bands are separated, we see that the density band makes the dominant contribution to $S(k_z)$ in the low- k_z limit. As k_z increases the phase band contribution increases, and $|\delta n_{\nu, k_z}|$ diverges for both the phase and density bands as $k_z \rightarrow 2\pi/L$.

The isothermal compressibility for the tube confined system can be defined as

$$\kappa = \frac{1}{n^2} \frac{\partial n}{\partial \mu}, \quad (16)$$

and relates to the number fluctuations of the system in a large measurement cell (e.g. see [51–53]). We determine this directly from the ground state calculations by evaluating how

⁴ In Sec. V we see that this behavior appears as a discontinuity in the compressibility, which is a second derivative of the thermodynamic potential.

⁵ For uniform state a finite peak occurs when the system has a roton, representing enhanced density fluctuations [43, 50]. This peak grows as the roton softens, and diverges when the roton energy goes to zero.

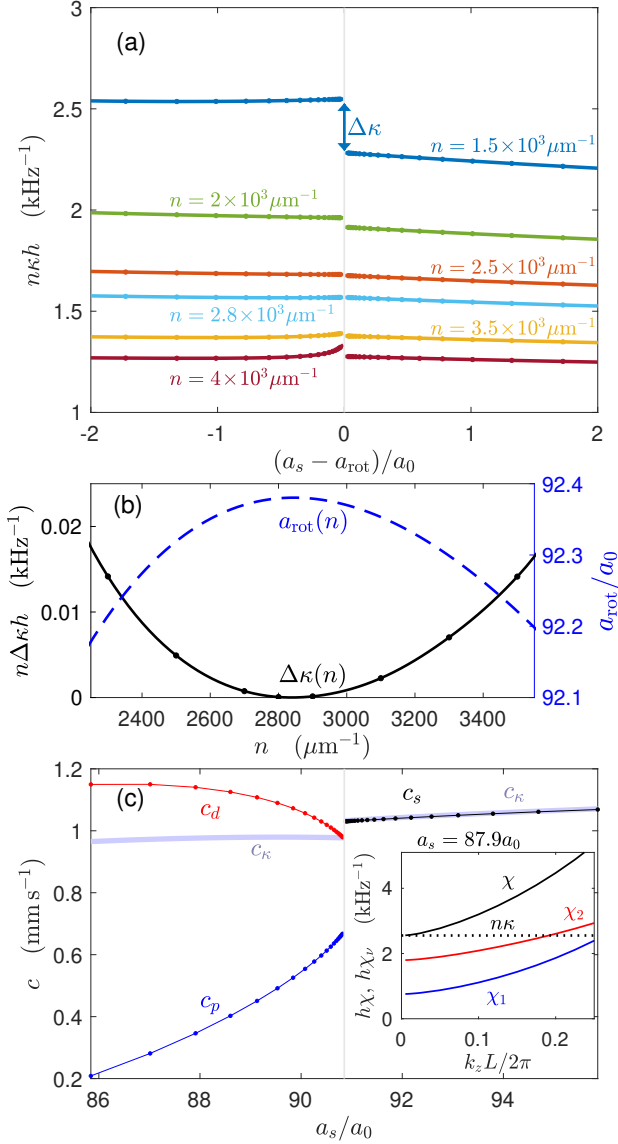


FIG. 4. (a) Compressibility across the transition for various linear densities. (b) The magnitude of the compressibility jump at the transition point (black line, with markers, left axes) compared to a_{rot} (blue dashed line, right axes) as a function of density. (c) For $n = 1.5 \times 10^3 \mu\text{m}^{-1}$ we show the speeds of sound (line and markers), compared against c_κ (blue solid line). Inset the contribution of the excitation branches to the compressibility sum rule for $a_s = 87.9 a_0$. Lowest (phase) excitation band (blue line), second density band (red line) and total of all bands (black line). Dotted horizontal line shows $n\kappa$ for reference. Other parameters as in Fig. 2.

the chemical potential changes with the average linear density. This expression directly relates to the speed of sound in the uniform system as

$$n\kappa = \frac{1}{mc_s^2}, \quad (17)$$

[43]. In Fig. 4(a) we show results for the compressibility

across the transition for systems of various densities. For reference the parameter range for the data in this subplot is indicated in the phase diagram in Fig. 1(b). The compressibility exhibits a discontinuous jump of $\Delta\kappa = \kappa^- - \kappa^+$ at the transition. Here κ^\pm denotes the compressibility at the transition approaching from the below (−) or above (+). Results for $\Delta\kappa$ are presented in Fig. 4(b), where we see that the discontinuity vanishes at $n \approx 2.85 \times 10^3 \mu\text{m}^{-1}$. We also show $a_{\text{rot}}(n)$ in this plot and observe that it is maximised around the same density value. The maximum in a_{rot} occurs from the competition between two-body interactions and the quantum fluctuation term [11]. The simultaneous occurrence of these extrema suggests that $\Delta\kappa$ vanishing is also related to this competition.

In Fig. 4(c) we consider the speeds of sound for a lower density case than the results presented in Fig. 3(b). For reference we have plotted the effective speed of sound

$$c_\kappa = \frac{1}{\sqrt{mn\kappa}}, \quad (18)$$

obtained assuming relationship (17) holds. We see that this value of c_κ agrees with c_s on the uniform side of the transition. In the modulated state it lies between the two speeds of sound, although at the transition its value coincides with c_d . This indicates that at the transition the phase branch does not contribute to the long wavelength density fluctuations of the system.

While the compressibility is calculated from the ground state chemical potential (16), we can link it to the excitations via dynamical structure factor using the relation

$$\int d\omega \frac{S(k_z, \omega)}{\omega} = \frac{1}{2} \chi(k_z), \quad (19)$$

where χ is the static density response function. From Eq. (13) we see that $\chi(k_z) = \sum_\nu \chi_\nu(k_z)$, where

$$\chi_\nu(k_z) \equiv \frac{2|\delta n_{\nu, k_z}|^2}{\epsilon_{\nu, q_z}}. \quad (20)$$

In the long-wavelength limit the compressibility sum rule [41, 54] is

$$\lim_{k_z \rightarrow 0} \chi(k_z) = n\kappa. \quad (21)$$

We verify that this relationship holds in the inset to Fig. 4(c). Similar to our treatment of the static structure factor in Figs. 2(a2)-(d2), we can examine the contribution of each of the gapless bands to (19), i.e. $\chi_{\nu=1,2}$. The results, shown in the inset to Fig. 4(c), reveal that in the modulated state the density and phase bands both significantly contribute to χ . The sum of these two saturates the contribution to χ for the range of k_z values shown in the inset. In contrast our earlier results showed that for low k_z the magnitude of $\delta n_{\nu, k_z}$ for the density band was significantly larger than the phase band⁶

⁶ The density band does not saturate the f-sum rule [41], but its contribution is much larger than the phase band.

[e.g. see Figs. 2(c2)-(d2)]. This behavior is different from the spin-orbit stripe phase case where the density band excitations (propagating parallel to the crystal) exhaust the compressibility sum rule [31]. The role of the phase band in increasing the compressibility relative to the density band was discussed in [9] for a 3D soft-core supersolid, although no direct comparison of the elementary excitations to the compressibility was made.

VI. CONCLUSIONS

In this paper we have studied the ground states and excitations of a dipolar BEC as it transitions to a supersolid state in an infinite tube potential. We have focused on the regime where the $D = 1$ crystalline order appears continuously, as characterized by the density contrast order parameter or the superfluid fraction. The compressibility and the speeds of sound obtained from the gapless energy bands are generally discontinuous across the transition, consistent with the transition being second order.

It is interesting to consider the prospects for measuring our predictions in experiments. Recent experiments with optical lattices have measured the speed of sound and determined the superfluid fraction using Bragg spectroscopy [55] and collective mode excitation [56]. These techniques could be applied to the dipolar system noting that Bragg spectroscopy has been used to measure the anisotropy of sound in a dipolar BEC [47], and to probe the free-particle excitations of a dipolar

supersolid [18]. Also, various forms of collective mode spectroscopy have already been demonstrated in this system [4–6, 16]. The compressibility relates to the number fluctuations in a large measurement cell [51–53] and has been measured experimentally in ultra-cold atoms experiments using *in-situ* density and density fluctuation measurements [57–60] (also see [61]). Related measurements have been performed in dipolar BECs and supersolids to determine the static structure factor [16, 49] and could be extended to probe compressibility.

ACKNOWLEDGMENTS

PBB acknowledges use of New Zealand eScience Infrastructure (NeSI) high performance computing facilities. PBB and DB acknowledge support from the Marsden Fund of the Royal Society of New Zealand. LC acknowledges support from the European Research Council (ERC) under the European Union’s Horizon Europe research and innovation program under grant number 101040688 (project 2DDip), and from the Deutsche Forschungsgemeinschaft (DFG, German Research Foundation) through project-ID 273811115 (SFB1225 ISOQUANT) and under Germany’s Excellence Strategy EXC2181/1-390900948 (the Heidelberg Excellence Cluster STRUCTURES). Views and opinions expressed are however those of the authors only and do not necessarily reflect those of the European Union or the European Research Council.

-
- [1] L. Tanzi, E. Lucioni, F. Famà, J. Catani, A. Fioretti, C. Gabbanini, R. N. Bisset, L. Santos, and G. Modugno, “Observation of a dipolar quantum gas with metastable supersolid properties,” *Phys. Rev. Lett.* **122**, 130405 (2019).
 - [2] Fabian Böttcher, Jan-Niklas Schmidt, Matthias Wenzel, Jens Hertkorn, Mingyang Guo, Tim Langen, and Tilman Pfau, “Transient supersolid properties in an array of dipolar quantum droplets,” *Phys. Rev. X* **9**, 011051 (2019).
 - [3] L. Chomaz, D. Petter, P. Ilzhöfer, G. Natale, A. Trautmann, C. Politi, G. Durastante, R. M. W. van Bijnen, A. Patscheider, M. Sohmen, M. J. Mark, and F. Ferlaino, “Long-lived and transient supersolid behaviors in dipolar quantum gases,” *Phys. Rev. X* **9**, 021012 (2019).
 - [4] L. Tanzi, S. M. Roccuzzo, E. Lucioni, F. Famà, A. Fioretti, C. Gabbanini, G. Modugno, A. Recati, and S. Stringari, “Supersolid symmetry breaking from compressional oscillations in a dipolar quantum gas,” *Nature* **574**, 382 (2019).
 - [5] Mingyang Guo, Fabian Böttcher, Jens Hertkorn, Jan-Niklas Schmidt, Matthias Wenzel, Hans Peter Büchler, Tim Langen, and Tilman Pfau, “The low-energy Goldstone mode in a trapped dipolar supersolid,” *Nature* **564**, 386 (2019).
 - [6] G. Natale, R. M. W. van Bijnen, A. Patscheider, D. Petter, M. J. Mark, L. Chomaz, and F. Ferlaino, “Excitation spectrum of a trapped dipolar supersolid and its experimental evidence,” *Phys. Rev. Lett.* **123**, 050402 (2019).
 - [7] Haruki Watanabe and Tomáš Brauner, “Spontaneous breaking of continuous translational invariance,” *Phys. Rev. D* **85**, 085010 (2012).
 - [8] T. Macrì, F. Maucher, F. Cinti, and T. Pohl, “Elementary excitations of ultracold soft-core bosons across the superfluid-supersolid phase transition,” *Phys. Rev. A* **87**, 061602 (2013).
 - [9] Francesco Ancilotto, Maurizio Rossi, and Flavio Toigo, “Supersolid structure and excitation spectrum of soft-core bosons in three dimensions,” *Phys. Rev. A* **88**, 033618 (2013).
 - [10] Santo Maria Roccuzzo and Francesco Ancilotto, “Supersolid behavior of a dipolar Bose-Einstein condensate confined in a tube,” *Phys. Rev. A* **99**, 041601 (2019).
 - [11] P Blair Blakie, D Baillie, and Sukla Pal, “Variational theory for the ground state and collective excitations of an elongated dipolar condensate,” *Commun. Theor. Phys.* **72**, 085501 (2020).
 - [12] P. B. Blakie, D. Baillie, L. Chomaz, and F. Ferlaino, “Supersolidity in an elongated dipolar condensate,” *Phys. Rev. Res.* **2**, 043318 (2020).
 - [13] Tobias Ilg and Hans Peter Büchler, “Ground-state stability and excitation spectrum of a one-dimensional dipolar supersolid,” *Phys. Rev. A* **107**, 013314 (2023).
 - [14] Joseph C. Smith, D. Baillie, and P. B. Blakie, “Supersolidity and crystallization of a dipolar Bose gas in an infinite tube,” *Phys. Rev. A* **107**, 033301 (2023).
 - [15] J. Hertkorn, F. Böttcher, M. Guo, J. N. Schmidt, T. Langen, H. P. Büchler, and T. Pfau, “Fate of the amplitude mode in a trapped dipolar supersolid,” *Phys. Rev. Lett.* **123**, 193002 (2019).
 - [16] J. Hertkorn, J.-N. Schmidt, F. Böttcher, M. Guo, M. Schmidt, K. S. H. Ng, S. D. Graham, H. P. Büchler, T. Langen, M. Zwier-

- lein, and T. Pfau, “Density fluctuations across the superfluid-supersolid phase transition in a dipolar quantum gas,” *Phys. Rev. X* **11**, 011037 (2021).
- [17] Giulio Biagioni, Nicolò Antolini, Aitor Alaña, Michele Modugno, Andrea Fioretti, Carlo Gabbanini, Luca Tanzi, and Giovanni Modugno, “Dimensional crossover in the superfluid-supersolid quantum phase transition,” *Phys. Rev. X* **12**, 021019 (2022).
- [18] D. Petter, A. Patscheider, G. Natale, M. J. Mark, M. A. Baranov, R. van Bijnen, S. M. Roccuzzo, A. Recati, B. Blakie, D. Baillie, L. Chomaz, and F. Ferlaino, “Bragg scattering of an ultracold dipolar gas across the phase transition from Bose-Einstein condensate to supersolid in the free-particle regime,” *Phys. Rev. A* **104**, L011302 (2021).
- [19] Zhen-Kai Lu, Yun Li, D. S. Petrov, and G. V. Shlyapnikov, “Stable dilute supersolid of two-dimensional dipolar bosons,” *Phys. Rev. Lett.* **115**, 075303 (2015).
- [20] Yong-Chang Zhang, Fabian Maucher, and Thomas Pohl, “Supersolidity around a critical point in dipolar Bose-Einstein condensates,” *Phys. Rev. Lett.* **123**, 015301 (2019).
- [21] Néstor Sepúlveda, Christophe Josserand, and Sergio Rica, “Nonclassical rotational inertia fraction in a one-dimensional model of a supersolid,” *Phys. Rev. B* **77**, 054513 (2008).
- [22] Yves Pomeau and Sergio Rica, “Dynamics of a model of supersolid,” *Phys. Rev. Lett.* **72**, 2426 (1994).
- [23] S. Sacconi, S. Moroni, and M. Boninsegni, “Excitation spectrum of a supersolid,” *Phys. Rev. Lett.* **108**, 175301 (2012).
- [24] C.-H. Hsueh, T.-C. Lin, T.-L. Horng, and W. C. Wu, “Quantum crystals in a trapped Rydberg-dressed Bose-Einstein condensate,” *Phys. Rev. A* **86**, 013619 (2012).
- [25] Masaya Kunimi and Yusuke Kato, “Mean-field and stability analyses of two-dimensional flowing soft-core bosons modeling a supersolid,” *Phys. Rev. B* **86**, 060510 (2012).
- [26] N. Henkel, R. Nath, and T. Pohl, “Three-dimensional roton excitations and supersolid formation in Rydberg-excited Bose-Einstein condensates,” *Phys. Rev. Lett.* **104**, 195302 (2010).
- [27] Jun-Ru Li, Jeongwon Lee, Wujie Huang, Sean Burchesky, Boris Shteynas, F Ç Top, Alan O. Jamison, and Wolfgang Ketterle, “A stripe phase with supersolid properties in spin-orbit-coupled Bose-Einstein condensates,” *Nature* **543**, 91 (2017).
- [28] Yun Li, Giovanni I. Martone, Lev P. Pitaevskii, and Sandro Stringari, “Superstripes and the excitation spectrum of a spin-orbit-coupled Bose-Einstein condensate,” *Phys. Rev. Lett.* **110**, 235302 (2013).
- [29] Yun Li, Lev P. Pitaevskii, and Sandro Stringari, “Quantum tricriticality and phase transitions in spin-orbit coupled Bose-Einstein condensates,” *Phys. Rev. Lett.* **108**, 225301 (2012).
- [30] Yun Li, Giovanni I. Martone, and Sandro Stringari, “Spin-orbit-coupled Bose-Einstein condensates,” in *Annual Review of Cold Atoms and Molecules* (World Scientific, 2015) Chap. 5, pp. 201–250.
- [31] Giovanni Italo Martone and Sandro Stringari, “Supersolid phase of a spin-orbit-coupled Bose-Einstein condensate: A perturbation approach,” *SciPost Phys.* **11**, 092 (2021).
- [32] Igor Ferrier-Barbut, Holger Kadau, Matthias Schmitt, Matthias Wenzel, and Tilman Pfau, “Observation of quantum droplets in a strongly dipolar Bose gas,” *Phys. Rev. Lett.* **116**, 215301 (2016).
- [33] L. Chomaz, S. Baier, D. Petter, M. J. Mark, F. Wächtler, L. Santos, and F. Ferlaino, “Quantum-fluctuation-driven crossover from a dilute Bose-Einstein condensate to a macrodroplet in a dipolar quantum fluid,” *Phys. Rev. X* **6**, 041039 (2016).
- [34] F. Wächtler and L. Santos, “Quantum filaments in dipolar Bose-Einstein condensates,” *Phys. Rev. A* **93**, 061603(R) (2016).
- [35] R. N. Bisset, R. M. Wilson, D. Baillie, and P. B. Blakie, “Ground-state phase diagram of a dipolar condensate with quantum fluctuations,” *Phys. Rev. A* **94**, 033619 (2016).
- [36] Aristeu R. P. Lima and Axel Pelster, “Quantum fluctuations in dipolar Bose gases,” *Phys. Rev. A* **84**, 041604 (2011).
- [37] D. Baillie, R. M. Wilson, and P. B. Blakie, “Collective excitations of self-bound droplets of a dipolar quantum fluid,” *Phys. Rev. Lett.* **119**, 255302 (2017).
- [38] A.J Leggett, “On the superfluid fraction of an arbitrary many-body system at $T = 0$,” *J. Stat. Phys.* **93**, 927 (1998).
- [39] L. Chomaz, R. M. W. van Bijnen, D. Petter, G. Faraoni, S. Baier, J. H. Becher, M. J. Mark, F. Wächtler, L. Santos, and F. Ferlaino, “Observation of roton mode population in a dipolar quantum gas,” *Nat. Phys.* **14**, 442 (2018).
- [40] Matthias Vojta, “Quantum phase transitions,” *Rep. Prog. Phys.* **66**, 2069 (2003).
- [41] Lev Pitaevskii and Sandro Stringari, *Bose-Einstein Condensation and Superfluidity*, Vol. 164 (Oxford University Press, 2016).
- [42] Masaya Kunimi, Yuki Nagai, and Yusuke Kato, “Josephson effects in one-dimensional supersolids,” *Phys. Rev. B* **84**, 094521 (2011).
- [43] Sukla Pal, D. Baillie, and P. B. Blakie, “Excitations and number fluctuations in an elongated dipolar Bose-Einstein condensate,” *Phys. Rev. A* **102**, 043306 (2020).
- [44] F. Zambelli, L. Pitaevskii, D. M. Stamper-Kurn, and S. Stringari, “Dynamic structure factor and momentum distribution of a trapped Bose gas,” *Phys. Rev. A* **61**, 063608 (2000).
- [45] P. B. Blakie, R. J. Ballagh, and C. W. Gardiner, “Theory of coherent Bragg spectroscopy of a trapped Bose-Einstein condensate,” *Phys. Rev. A* **65**, 033602 (2002).
- [46] M. Krämer, C. Menotti, L. Pitaevskii, and S. Stringari, “Bose-Einstein condensates in 1d optical lattices,” *Eur. Phys. J. D* **27**, 247–261 (2003).
- [47] G. Bismut, B. Laburthe-Tolra, E. Maréchal, P. Pedri, O. Gorceix, and L. Vernac, “Anisotropic excitation spectrum of a dipolar quantum Bose gas,” *Phys. Rev. Lett.* **109**, 155302 (2012).
- [48] D. Petter, G. Natale, R. M. W. van Bijnen, A. Patscheider, M. J. Mark, L. Chomaz, and F. Ferlaino, “Probing the roton excitation spectrum of a stable dipolar Bose gas,” *Phys. Rev. Lett.* **122**, 183401 (2019).
- [49] J.-N. Schmidt, J. Hertkorn, M. Guo, F. Böttcher, M. Schmidt, K. S. H. Ng, S. D. Graham, T. Langen, M. Zwerlein, and T. Pfau, “Roton excitations in an oblate dipolar quantum gas,” *Phys. Rev. Lett.* **126**, 193002 (2021).
- [50] P. B. Blakie, D. Baillie, and R. N. Bisset, “Roton spectroscopy in a harmonically trapped dipolar Bose-Einstein condensate,” *Phys. Rev. A* **86**, 021604 (2012).
- [51] M. Klawunn, A. Recati, L. P. Pitaevskii, and S. Stringari, “Local atom-number fluctuations in quantum gases at finite temperature,” *Phys. Rev. A* **84**, 033612 (2011).
- [52] R. N. Bisset and P. B. Blakie, “Fingerprinting rotons in a dipolar condensate: Super-poissonian peak in the atom-number fluctuations,” *Phys. Rev. Lett.* **110**, 265302 (2013).
- [53] D. Baillie, R. N. Bisset, C. Ticknor, and P. B. Blakie, “Number fluctuations of a dipolar condensate: Anisotropy and slow approach to the thermodynamic regime,” *Phys. Rev. Lett.* **113**, 265301 (2014).
- [54] S. Stringari, “Sum rules and Bose-Einstein condensation,” in *Bose-Einstein Condensation*, edited by A. Griffin, D. W. Snoke, and S. Stringari (Cambridge University Press, 1995) p. 86–98.
- [55] Junheng Tao, Mingshu Zhao, and Ian Spielman, “Observation of anisotropic superfluid density in an artificial crystal,” (2023),

- arXiv:2301.01258.
- [56] G. Chauveau, C. Maury, F. Rabec, C. Heintze, G. Brochier, S. Nascimbene, J. Dalibard, J. Beugnon, S. M. Rocuzzo, and S. Stringari, “Superfluid fraction in an interacting spatially modulated bose-einstein condensate,” *Phys. Rev. Lett.* **130**, 226003 (2023).
- [57] Nathan Gemelke, Xibo Zhang, Chen-Lung Hung, and Cheng Chin, “In situ observation of incompressible Mott-insulating domains in ultracold atomic gases,” *Nature* **460**, 995 (2009).
- [58] Chen-Lung Hung, Xibo Zhang, Nathan Gemelke, and Cheng Chin, “Observation of scale invariance and universality in two-dimensional Bose gases,” *Nature* **470**, 236 (2011).
- [59] Mark J. H. Ku, Ariel T. Sommer, Lawrence W. Cheuk, and Martin W. Zwierlein, “Revealing the superfluid lambda transition in the universal thermodynamics of a unitary Fermi gas,” *Science* **335**, 563 (2012).
- [60] Ye-Ryoung Lee, Myoung-Sun Heo, Jae-Hoon Choi, Tout T. Wang, Caleb A. Christensen, Timur M. Rvachov, and Wolfgang Ketterle, “Compressibility of an ultracold Fermi gas with repulsive interactions,” *Phys. Rev. A* **85**, 063615 (2012).
- [61] F. J. Poveda-Cuevas, P. C. M. Castilho, E. D. Mercado-Gutierrez, A. R. Fritsch, S. R. Muniz, E. Lucioni, G. Roati, and V. S. Bagnato, “Isothermal compressibility determination across Bose-Einstein condensation,” *Phys. Rev. A* **92**, 013638 (2015).